

1 Active acquisition for multimodal neuroimaging

2
3
4
5
6
7 ‡ Department of Neuroimaging, Institute of Psychiatry, Psychology and Neuroscience, King's College
8 London, London, UK.

9 § MRC Centre for Cognition and Brain Sciences, University of Cambridge, Cambridge, UK; Max
10 Planck Institute for Human Cognitive & Brain Sciences, Leipzig, Germany.

11 ¶ Faculty of Medicine, Department of Medicine, Imperial College London, London, UK.
12

13 Abstract

14 In many clinical and scientific situations the optimal neuroimaging sequence may not be known prior
15 to scanning and may differ for each individual being scanned, depending on the exact nature and
16 location of abnormalities. Despite this, the standard approach to data acquisition, in such situations, is
17 to specify the sequence of neuroimaging scans prior to data acquisition and to apply the same scans to
18 all individuals. In this paper, we propose and illustrate an alternative approach, in which data would
19 be analysed as it is acquired and used to choose the future scanning sequence: active acquisition. We
20 propose three active acquisition scenarios based around multiple MRI modalities. In Scenario 1, we
21 propose a simple use of near-real time analysis to decide whether to acquire more or higher resolution
22 data or acquire data with a different field-of-view. In Scenario 2, we simulate how multimodal MR
23 data could be actively acquired and combined with a decision tree to classify a known outcome variable
24 (in the simple example here, age). In Scenario 3, we simulate using Bayesian optimisation to actively
25 search across multiple MRI modalities to find those which are most abnormal. These simulations
26 suggest that by actively acquiring data, the scanning sequence can be adapted to each individual. We
27 also consider the many outstanding practical and technical challenges involving normative data
28 acquisition, MR physics, statistical modelling and clinical relevance. Despite these, we argue that by
29 active acquisition allows for potentially far more powerful, sensitive or rapid data acquisition and may
30 open up different perspectives on individual differences, clinical conditions and biomarker discovery.

31

32

33 **Introduction**

34 Neuroimaging involves trade-offs; whether for clinical diagnosis, patient stratification or biomarker
35 discovery. For example, with a typical MRI scan, there are substantial practical constraints (money,
36 patient comfort and compliance, radiological reporting) which means decisions have to be taken as to
37 what kind of scan to perform, where in the brain scan, the scan resolution. The standard approach is to
38 make these decisions before scanning commences, acquiring the data then analysing it. However, the
39 optimal resolution/type of scan will depend on what is being investigated and the type and the location
40 of pathology or abnormalities and may not be known *a priori*.

41 Here, we propose an alternative approach using active learning for real-time optimisation of
42 neuroimaging data acquisition; providing illustrative examples. Broadly, in our approach data
43 acquisition and analysis are not separated; instead data is analysed as it is acquired and used to guide
44 subsequent data acquisition, in a closed-loop. The word game *hangman* is a simple illustration of a
45 form of active learning (as is predictive text messages and search engine auto-completion): a letter is
46 guessed, and whether it is present or not is then evaluated; this information is then used to narrow the
47 search for the next letter. Active learning approaches are potentially far more efficient (in terms of
48 scanner time) than treating acquisition and analysis as separate phases. A non-active learning version
49 of hangman would involve guessing all the letters at the start of the game and then evaluating them all
50 at once without any feedback; in most situations, this would be a highly inefficient strategy.

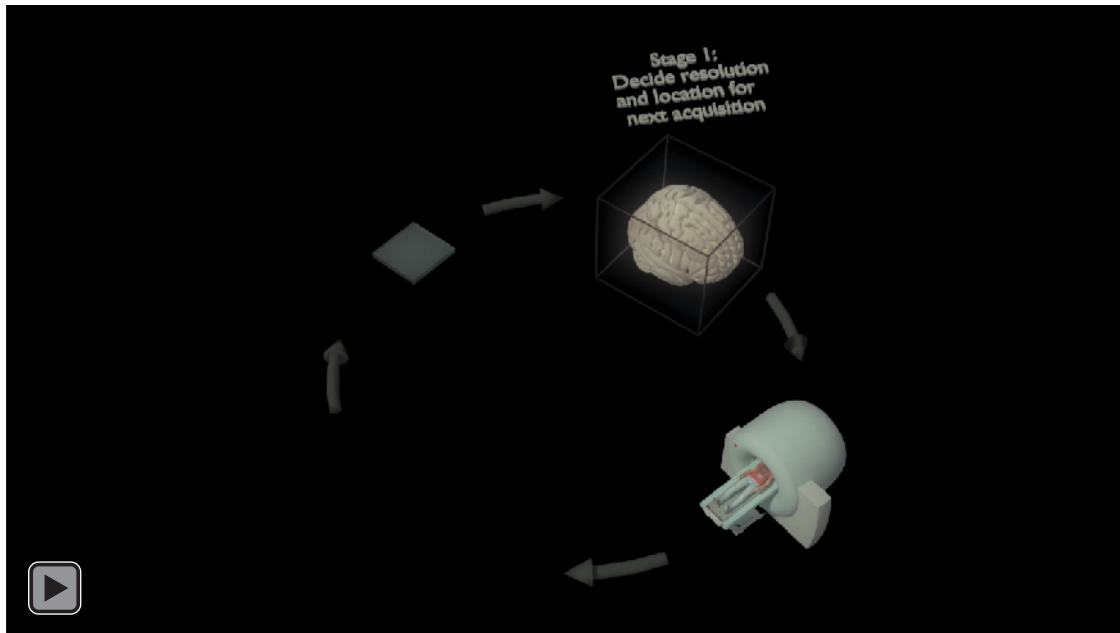
51 We have previously demonstrated that active learning can be used to guide the choice of experimental
52 paradigm in functional MRI (Lorenz et al. 2016): with substantial increases in terms of speed,
53 searching over many experimental parameters far quicker than an exhaustive search. This allows for
54 far broader research questions to be asked (Lorenz et al. 2018). Active learning also has another
55 important feature; they involve a prediction and testing cycle, with the learner having to make
56 predictions that are then tested with out-of-sample data. This potentially increases the replicability of
57 analyses and reduces the ability for post-hoc bias (Lorenz, Hampshire, and Leech 2017; Lancaster et
58 al. 2018).

59 The work presented here investigates the use of sequential decision-making to select the type of scan,
60 using information gained from previous scans actively seek out brain abnormalities or make diagnostic
61 predictions. This requires data to be collected and analysed in near real-time; however, to illustrate the
62 potential power of this approach our demonstrations use previously collected data, by simulating the
63 real-time analysis aspect.

64 Figure 1 presents a video overview of Active Acquisition: (i) scan parameters are chosen (e.g.,
65 modality or acquisition parameters such as resolution, TR or TE); (ii) the scan is acquired; (iii) pre-
66 processed; and, (iv) acquired data is compared to an existing normative dataset. The loop then
67 continues with the information in (iv) used to optimise the next scan (or decide whether sufficient data

68 have been collected to stop scanning). We explore using Active Acquisition in three different scenarios
69 with T1-weighted MR images:

- 70 1) Finding a localised structural anomaly (e.g., locating a focal lesion).
71 2) Choosing the optimal scanning modality to actively detect abnormalities.
72 3) Actively choosing the type of scan to characterize an aspect of the individual being scanned
73 (e.g., age).



74

75 Figure 1: General illustrative video of one active acquisition approach for structural neuroimaging. (The video may
76 not work with some PDF viewers).

77 **Methods**

78 **Scenario 1: Changing structural scan resolution to detect stroke pathology**

79 Our rationale is to start at a low image resolution for a (very rapid) whole brain scan, before acquiring
80 higher resolution scans if the brain appears to be abnormal. This way, it is possible to efficiently image
81 a focal pathology such as a lesion or tumour and to rapidly estimate its spatial location and establish
82 whether more data needs to be acquired, potentially with a restricted field of view focused on the site
83 of the abnormality. Supporting Matlab code can be found in supplementary material.

84 *Choice of scan parameters*

85 For our illustrative simulation, we used existing structural scans (though in practice they would be
86 acquired and analysed online). Practical challenges and limitations to acquiring these data, as well as
87 consider possible methods to mitigate these challenges, as outlined in the Discussion section.

88 At each iteration, the scan is divided into three equally sized volumes, along the z-dimension. The
89 ‘outlier distance’ (defined below) is then quantified for each third by reference to the distribution in
90 an independent normative sample. The volume with the highest outlier distance is then selected and
91 the next scan “acquired”; covering same section of the volume but with the resolution doubled. The
92 process was repeated three times until the maximum resolution of 1mm³ voxel was achieved. The
93 choice of resolution and number of sub-divisions (and other scanner parameters) presented in this
94 scenario is relatively arbitrary. Future work will need to establish the optimal approach for a given
95 clinical or scientific question. There will always be a trade-off between multiple comparisons and
96 precision when assessing; here we chose a very coarse approach which should be sufficient, given the
97 focal and macroscopic nature of the brain injury (i.e., lesion). In clinical or scientific applications, a
98 more sophisticated approach would probably be required, that chooses the brain region for the outlier
99 detection (and potentially subsequent more targeted acquisition), related to the size and location of the
100 pathology or abnormality, possibly changing orientation and the image field-of-view in the process.

101 *Outlier distance from normative sample*

102 The extent to which a participant's image was different from the normative sample was quantified,
103 restricted to the resolution and coverage of the specific scan. The median distance between an
104 individual's scan and each participant in the normative dataset was calculated using the median
105 absolute deviation (in Euclidean distance) of signal intensity averaged across all voxels. This results
106 in a single value of outlier distance. The choice of outlier quantification depends on the type of data
107 being acquired and the question being asked. We opted for the median absolute deviation because it is
108 a simple measure that is relatively robust to violations of normality assumptions. However, we note
109 that many other more sensitive outlier measures could also be used (e.g., measures taking into account
110 covariance across voxels, Fritsch et al. 2012).

111 **Scenario 2: Active multimodal stratification of individual differences**

112 In this scenario, Active Acquisition is used to choose the modality of the scan to achieve a given goal.
113 The rationale is that the optimal scanning modality for assessing an individual, for example to quantify

their relationship to a normative sample, will vary for different individuals; when performing a battery of scans, each individual may have a different set of scans and a different acquisition order.

In Scenario 2, we use multimodal imaging to quantify individual variability. This type of analysis could be relevant when classifying or stratifying individuals into scientifically or clinically relevant groups. To illustrate this, we use the Cam-CAN dataset (Shafto et al. 2014) and with the task of predicting chronological age from neuroimaging data. Predicting age is a useful example case for active multimodal imaging because there are large datasets available, there is little ambiguity about label validity (unlike many clinical descriptions), age is associated with large-scale neural changes (e.g., Good et al. 2001) and “brain-predicted age” has been shown to relate to many other health related biomarkers (e.g., Cole et al. 2018). Cam-CAN is a particularly useful dataset to assess this source of individual variability since the age distribution of the participants is approximately equally balanced across seven decades from 20s to 80s.

To instigate Active Acquisition in this case, we simulate active learning process by fitting a decision tree regression model to the six modalities of Cam-CAN; predictions of chronological age were the outcome measure. This is because: a low-depth decision tree would not include all modalities, just those important for predicting age; makes the decision sequentially (i.e., modality by modality) rather than simultaneously, thus is well-suited for Active Acquisition, and finally; allows different individuals to have different scans and different orders of scans.

A holdout dataset was created with 20% of the individuals, selected randomly (the data partition was performed once rather than pooling across multiple, randomly generated partitions). A decision tree was fit to the remaining 80% of individuals’ six imaging modalities as the predictor variables and their ages in years as the outcome variable. The model hyper-parameters (tree depth, number of leaves, etc.) were estimated with Bayesian optimisation (see supplementary material for Matlab code). Subsequently, the decision tree was evaluated with the holdout participants. The application of the decision tree (the sequential decision process) to each individual in the holdout group, could be performed in real-time to new participants in exactly the same way. For comparison, we also fit a standard support vector regression, with hyper-parameters also optimised with Bayesian optimisation, to the same data (see Matlab code) which used all data modalities simultaneously.

Scenario 3: Active discovery of individual differences with multi-modal imaging

Whereas Scenario 2 focuses on quantifying how an individual varies along some dimension (e.g., age), in Scenario 3, we attempt to actively learn which modality an individual is most likely to be an outlier in. This could be useful for efficiently finding pathology in an individual or for discovering biomarkers; particularly, when there are a large number of possible modalities to choose from and a limited amount of scanning time/participant tolerance of scanning (see supplementary material for code).

To illustrate Scenario 3, we again used the Cam-CAN dataset, as per Scenario 2. In addition, we included a Bayesian optimisation algorithm (Shahriari et al. 2016) to actively learn which modality is most abnormal (as quantified by the magnitude of outlier measurement). Bayesian optimisation is

152 particularly well suited for this type of problem when the objective underlying function is unknown
153 and costly to evaluate and relatively robust to the presence of noise in the data.

154 For optimisation to work efficiently, the acquisition function needs to take advantage of existing
155 information; in this case the covariance across individuals for different modalities. Therefore, we split
156 the data into two: 80% of the Cam-CAN participants were used to estimate the space (across
157 modalities) for the algorithm to search across. To do this, we converted each modality to a z-score,
158 then performed a factor analysis (using Matlab) and calculated a single factor. We then reorganized
159 the modalities for the search space for the Bayesian optimisation in terms of weighting on the principle
160 factor; this process estimates how different modalities will co-vary (approximately) with each other.
161 For this example, with only six modalities to choose from, we opted for a simple experiment space
162 with modalities given an integer between 1-6, based on the output of the factor analysis and the
163 optimisation algorithm output integers. For more realistic situations with more complicated spaces
164 (e.g., with many modalities organised along multiple dimensions and with more continuous
165 modalities) one could use alternative (e.g., ratio) scales.

166 Subsequently, we performed Bayesian optimisation using the remaining 20% of participants, allowing
167 the algorithm to pick the modality for a given individual, with the target objective of finding the
168 minimum z-score. Given the relatively small number of available modalities, we allowed the algorithm
169 to randomly choose three modalities (the burn-in phase) to sample first, to fit a Gaussian process
170 regression and then to use the expected-improvement acquisition function to choose the next point to
171 sample. The expectation was that after some initial random exploration, the model should be able to
172 take advantage of the covariance across individuals to estimate the modality with the minimum z-score
173 more frequently than expected by chance.

174 To assess whether this optimisation approach was performing above chance levels, we compared
175 results for each individual with the correct factor ordering of modality (based on the covariance
176 structure across individuals) with a random ordering of modalities. For each individual the order of
177 the modalities was randomised (i.e., the ordering of the modalities was no longer based on prior
178 information about how individuals co-vary across modalities). For both random and true covariance
179 models, we calculated the proportion of participants where the optimisation algorithm correctly found
180 the minimum z-score modality. This assessment process was repeated 100 times with different random
181 seeds, allowing different burn-in sampling trajectories for each individual for each iteration.

182 Data acquisition

183 In Scenario 1, data were acquired from 13 participants: seven healthy controls with no history of
184 neurological problems (average age= 56, range = 46 to 67, female=4); and, six patients with chronic
185 left-hemisphere middle-cerebral artery focal strokes (average age= 60, range = 47 to 78, female=2,
186 average lesion volume= 10.6 cm³). For each participant, three T1-weighted scans were acquired at
187 different voxel resolutions: 1mm³, 2mm³, 4mm³. As with other data presented here, the patient and
188 control data were not collected in real-time but is intended to illustrate the general utility of the
189 approach. In this example, we use seven healthy controls as a “normative” sample; this is, obviously,

190 far too small for actual practical uses, but was limited by the data set available (multiple resolutions
191 per individual) but does illustrate the potential of the approach if scaled-up.

192 For Scenarios 2 and 3, multimodal MRI data from 611 people (age range from 18-88, 312, female)
193 were taken from the Cam-CAN dataset. This data consisted of T1-weighted, T2-weighted, diffusion-
194 weighted MRI, three functional scans (resting-state fMRI, movie-watching fMRI and a blocked
195 sensorimotor task-based fMRI). Imaging acquisition has been presented in detail elsewhere (Shafto et
196 al. 2014).

197 **Image pre-processing**

198 *Scenario 1:*

199 To explore the feasibility of processing brain images in near real-time and to make minimal
200 assumptions about the location or nature of pathology when calculating outlier distance, we used very
201 simple and rapid pre-processing. T1-weighted images were converted from DICOM to NifTI format
202 before being linearly-registered into MNI152 1mm³ space using the very efficient registration tool
203 NiftyReg (Modat 2012). The same process was performed for each of the three different image
204 resolutions acquired.

205 *Scenario 2 & 3:*

206 *T1-weighted MRI*

207 All T1-weighted structural images from all three datasets were processed in the same way as follows.
208 Grey matter (GM), white matter (WM) and cerebrospinal fluid (CSF) volumes were calculated using
209 SPM12 ‘Segment’ (University College London, UK). Voxelwise assessment of changes to brain
210 volume was calculated using the SPM symmetric diffeomorphic registration process (Ashburner 2007)
211 to a predefined template used in our previous studies (Cole et al. 2018).

212 For the Cam-CAN dataset, the other modalities were (briefly) processed as detailed below. These
213 analyses are merely illustrative of the type of data that could be extracted; they have been simplified
214 from multivariate raw data for each individual into a single summary statistic, chosen for its simplicity
215 rather than because it is optimal for measuring individual variability.

216 *Diffusion-weighted MRI*

217 White-matter microstructure was analysed under the diffusion tensor imaging (DTI) paradigm, using
218 FSL (<http://fsl.fmrib.ox.ac.uk/>) tract-based spatial statistics (Smith et al. 2006) with DTI-TK (Zhang
219 et al. 2007) software for affine then non-linear tensor-based image registration. Normalised tensor
220 images were used to derive voxelwise measures of fractional anisotropy (FA) and mean diffusivity.

221 Mean values across major WM fibre tracts, taken from the JHU-ICBM tract atlas, were calculated,
222 resulting in an FA average value per individual.

223 *T2-weighted MRI*

224 The same diffeomorphic transformation that was calculated for the grey matter was applied to the T2-
225 weighted scan data to warp each individual's data into the same T1-weighted template space.
226 Subsequently, the average T2-weighted intensity values from the normalised image was calculated.

227 *Resting state functional connectivity*

228 Measures of 'within-network' connectivity were calculated from resting-state fMRI data using FSL
229 'Dual Regression' (Filippini et al. 2009). Prior to the dual regression, standard FSL 'MELODIC'
230 analysis pipeline was applied (Smith et al. 2004): high-pass temporal filtering at 100s, spatial
231 smoothing at 5mm FWHM, global intensity normalisation, motion-correction followed by realigning
232 the data into MNI152 space using linear registration before the data were resampled into 4x4x4mm
233 voxel space. Then the data were cleaned by linearly regressing six motion parameters from each
234 voxel's time-course, before nuisance WM and CSF time-courses were linearly regressed from each
235 voxel (using average CSF and WM masks from the segmentation). Subsequently, using canonical
236 spatial maps of twenty networks (including both intrinsic connectivity networks and likely noise
237 networks) (Smith et al. 2009), cleaned data underwent a multiple regression to derive voxelwise
238 measures of connectivity for each network for each individual. Finally, to keep this aspect of the
239 approach as simple as possible, we averaged all voxels within the default mode network (DMN) mask;
240 this process resulted in an individualized 'within-network' connectivity measure for the DMN. Future
241 work (with any fMRI data) could explore only using short segments of the functional time-series
242 (rather than the whole scan), to allow for faster, repeated measurements.

243 *Movie-watching functional connectivity*

244 This was identical to the analysis of the resting state connectivity, calculating individualised within-
245 DMN functional connectivity while watching the movie.

246 *Task fMRI*

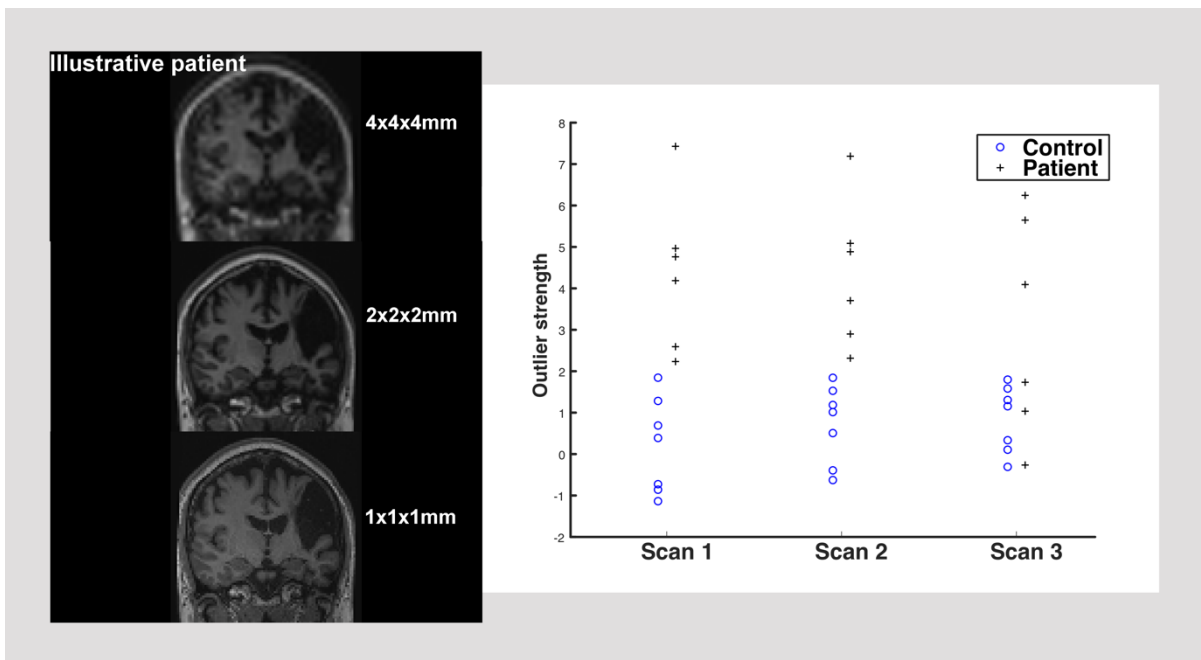
247 The sensorimotor task data were analysed following a standard FSL pipeline: global intensity
248 normalisation, high-pass temporal filtering at 100s, spatial smoothing at 5mm FWHM, motion-
249 correction, registration of the data into MNI152 space using linear registration. Subsequently, a general
250 linear model was applied voxelwise (using the standard FSL approach for dealing with the auto-
251 correlation of residuals (Smith et al. 2004)), with separate explanatory variables modelling auditory
252 and visual blocks convolved with a canonical hemodynamic response function. Subsequently, a
253 contrast of all task conditions versus the implicit baseline was calculated and a higher-level group
254 mixed-effects model was used to calculate increased and decreased BOLD activity with task. This
255 resulted in group task positive and task negative networks which were converted into binary mask
256 defined by voxels that survived cluster correction for multiple comparisons. An individualised task

257 fMRI measure was calculated by taking the average activity within the positive network mask and
 258 subtracting the average value from the negative network mask.

259 **Results**

260 **Scenario 1: Changing structural scan resolution to detect stroke pathology**

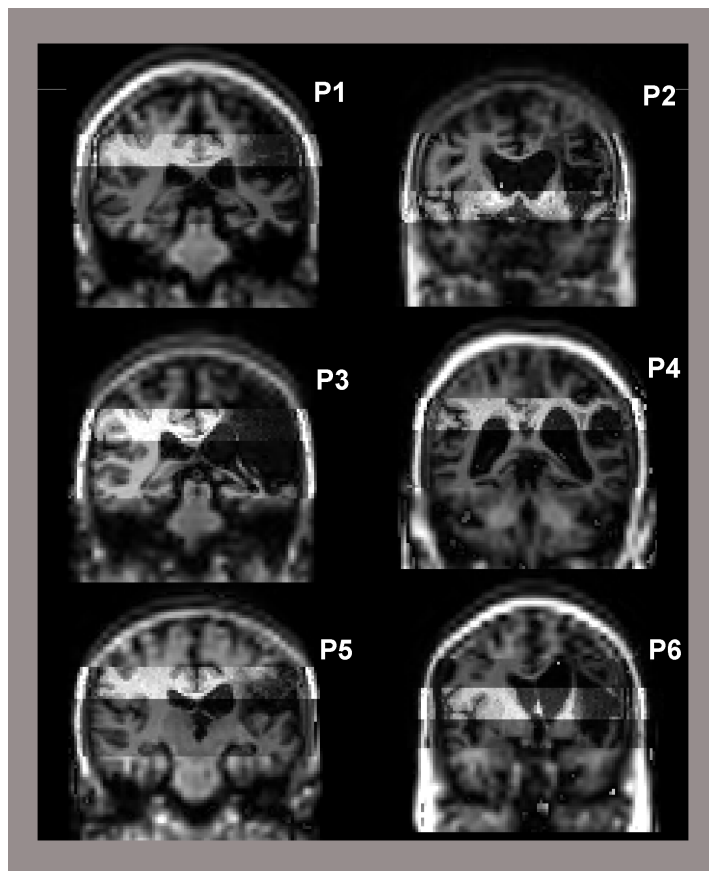
261 The simplest Active Acquisition model involves starting with a rapid, low resolution structural scan,
 262 analysing it and then deciding to whether to acquire further higher-resolution scan(s). Here, we
 263 collected lower-resolution (4mm^3) structural scans from six patients with focal brain lesions and seven
 264 age-matched controls, followed by intermediate-resolution (2mm^3) and higher-resolution (1mm^3)
 265 scans. An illustrative patient at three resolutions is presented in Figure 1 (left). Even with the lowest
 266 resolution scan, patients and control participants (Figure 1 - right) show a large difference in terms of
 267 outlier distance. This example, in patients with large focal strokes, illustrates how data simple
 268 measures calculated in near real time, and then a decision made as to whether a slower, higher
 269 resolution scan is needed or not. As can be seen from the outlier measurements, only a subset of the
 270 control participants, close to the boundary with the patients would require slower, additional scans.



271
 272 Figure 2: Left, a stroke patient with three different resolution T1-weighted scans. Right, outlier distance from
 273 control participants, for each participant for the three different scans, and combining all three scans. For each
 274 scan, the scan is subdivided into three, and the maximum outlier distance (out of the three subdivisions assessed)
 275 from the control data is plotted. This shows a relatively clear difference in outlier distance between patients and
 276 controls. For most patients and controls (either far from 0 or close to 0 respectively), there is no need to collect
 277 additional higher resolution (slower) scans to differentiate the two groups.

278 We also simulated optimising the scan field-of-view in near-real-time. In this case, at each resolution
 279 the brain is divided into thirds and the negative outlier distance calculated for each third. The third that
 280 is most strongly classed as an outlier is then retained and subsequent, higher resolution scans, acquired
 281 just within that third. The process then repeats (Figure 3, top). This illustrates how a composite brain

282 image can be built up out of increasing resolution scans. This could trade-off sensitivity for tissue
 283 contrast with increasing quantification of brain structure, while limiting scanning time.



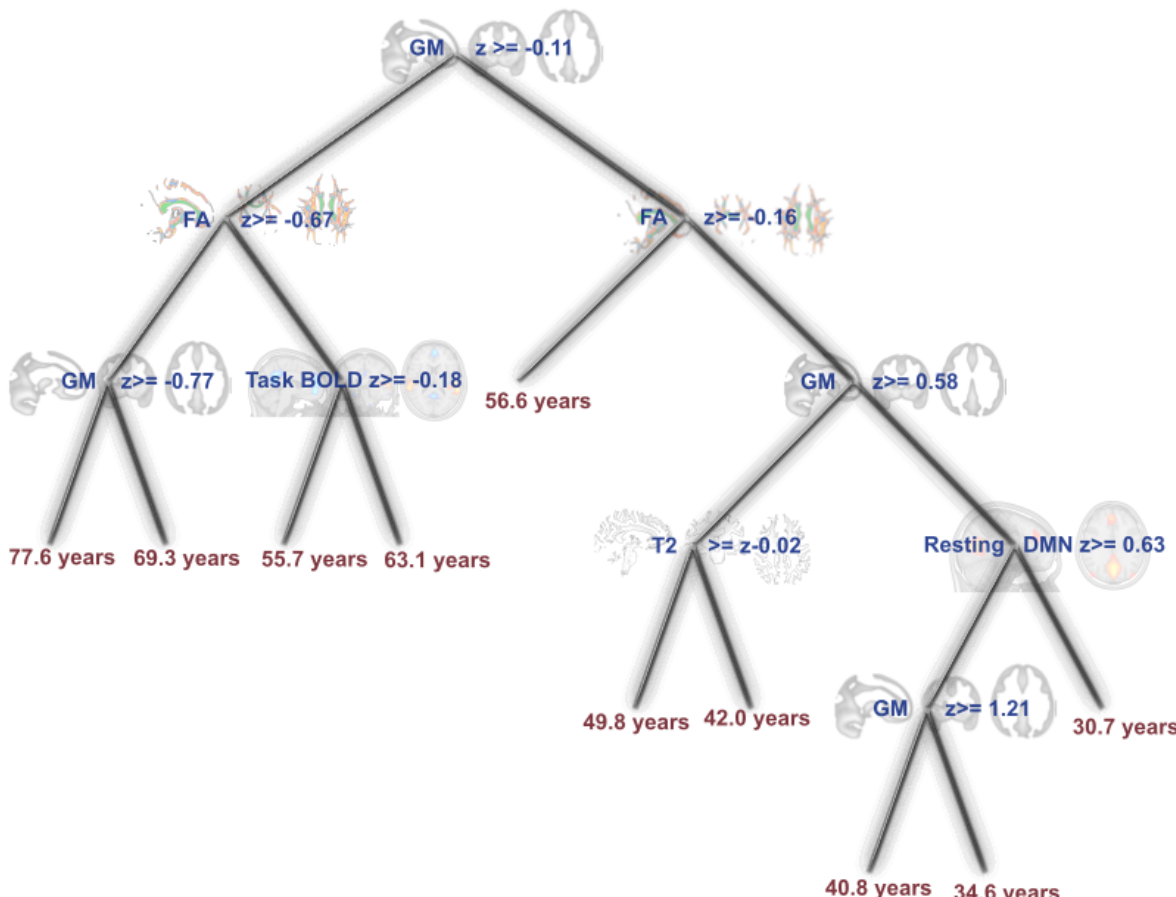
284
 285 Figure 3: top, composite coronal slices (one for each of the six patients), built out of increasing resolution with
 286 different coverage T1-weighted scans, restricting the scan volume to that quantified as most abnormal relative
 287 to the controls. This demonstrates that the very simple approach to subdividing the brain and quantifying outliers
 288 can be used to ‘zoom’ in on areas of pathology that are specific for individual patients.

289 Scenario 2: Active multimodal stratification of individual differences

290 When fitting the decision tree regression to predict chronological age from neuroimaging data, the
 291 regression model contained multiple modalities (indicating its utility in a sequential acquisition and
 292 analysis procedure). It started with GM volume, consistent with previous data suggesting a strong
 293 relationship between GM and age (Good et al. 2001), with lower z-scores indicating older age.
 294 Subsequently, average WM FA was chosen, again with lower values relating to older age. Next, the
 295 model’s branches become very different, both in terms of modality chosen and number of scans
 296 required, depending on the route through the tree.

297 We observed that the mean absolute error (MAE) of age prediction is 10.47 years and the median error
 298 8 years. For comparison, the MAE calculated on the same data using a support vector regression
 299 approach with all of the data is very similar, was 10.42 years, with a median error of 9.4 years. The
 300 predicted age performance is considerably worse than has been reported elsewhere for single
 301 modalities from the same dataset e.g., (Lancaster et al. 2018); this is to be expected given that, for
 302 illustrative simplicity, we have collapsed large, multivariable datasets into single summary statistics
 303 (i.e., a single value for grey matter probability per individual etcetera). In practice, sequential

304 decision methods incorporating multivariate datasets to utilise the full richness of the underlying data
 305 are needed to realise the potential of the approach.



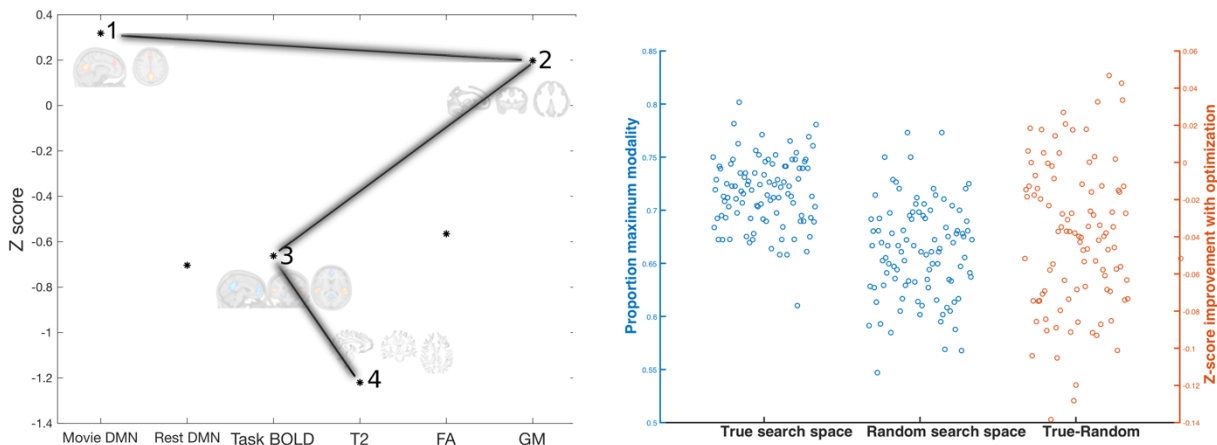
306
 307 Figure 4: The decision tree regression model calculated on summary statistics for each of six modalities to
 308 predict individual age. At each node in the tree the z-scored data for a given individual are used to decide
 309 modality to use next or whether to stop at this point. This can happen in near-real time, with different individuals
 310 taking different routes through the tree, and with different numbers of scans. The estimated age is then
 311 approximated by the age at the leaf nodes.

312 Scenario 3: Active discovery of individual differences with multi-modal imaging

313 Here we simulated closed-loop Bayesian optimisation used to discover the modality for a given
 314 individual (from the holdout dataset) where the negative outlier distance is most (i.e., relative to
 315 normative data from the training dataset), shown in Figure 5. For the optimisation to work efficiently
 316 (i.e., faster than exhaustive search across modalities), it needs to take advantage of covariance across
 317 modalities in individual differences. In Figure 5A, the order of modalities (Movie, Rest, Task, T2, FA,
 318 GM) reflects this covariance structure. This provides prior information that the optimisation algorithm

319 can combine with some random initial samples (numbers 1-3 in Figure 5A, left) to build a Gaussian
 320 process regression model to predict the modality with minimum z-score (in this case number 4, T2).

321 By chance, the proportion of participants for whom the algorithm finds the modality with the minimum
 322 z-score is 0.67 (given that it sampled four modalities in total). When the Bayesian optimisation
 323 algorithm utilises the estimated covariance structure from the training dataset, the proportion increases
 324 to >0.72 on average (results in Figure 5B are presented from 100 replications). We see that if the
 325 modality ordering is chosen randomly (rather than based on covariance across individuals from the
 326 training set) the average proportion of participants where the minimum modality is selected
 327 approximates that expected by chance (i.e., 0.67). We also see that this translates into an increase in
 328 the estimated minimum z-score found when using the optimisation algorithm compared to the random
 329 modality ordering. This difference between true and random ordering of modality search space is
 330 relatively modest (approximately 5%). However, the dataset used in this example has very few
 331 modalities and thus a restricted search space and has a relatively limited sample size. Also, we used
 332 somewhat coarse pre-processing and summary statistics. Applying this approach to on-going data
 333 collection in much larger projects or at clinical neuroimaging centres that scan large numbers of
 334 people, alongside the myriad of different MRI scan modalities available, means that this approach
 335 could be substantially improved and used much more powerfully for biomarker discovery.



336

337 Figure 5: Active discovery of individual differences across modalities, controlled by a closed-loop optimisation
 338 algorithm. Left, the trajectory of the algorithm as it traverses the modality space, estimating a model of which
 339 modalities a specific individual appears most abnormal in, without exhaustively sampling every point, before
 340 guessing which is the most abnormal. Right, proportion of participants in the holdout set where the optimisation
 341 algorithm correctly chose the modality most sensitive to abnormalities for both true and random modalities, and

342 the decrease in estimated minimum z-statistic for true versus random organisation of modalities (repeated 100
343 times with different burn-in random initialisation of the models).

344 **Discussion**

345 Here we outlined the Active Acquisition approach for optimising multimodal neuroimaging scan
346 protocols. The examples are intended to illustrate the potential utility of Active Acquisition; by using
347 this approach important decisions about the scan do not need to be in advance; how long to scan for,
348 what modalities to acquire, which regions of the brain to focus on. Rather, the precise nature of the
349 scanning protocol is determined online, adapting to the individual in the scanner, optimising
350 acquisition for a given set of circumstances. Our current goal has been to outline several broad
351 scenarios that suggest how Active Acquisition could progress and its general potential, rather than
352 provide evidence of a specific biomarker or indeed specific pipelines or analysis approaches. Here, we
353 discuss future potential directions for Active Acquisition, in particular for diagnosis and stratification
354 as well as for biomarker discovery. We envisage these two directions developing along independent
355 but complementary lines. We also consider some practical issues that need to be overcome to take the
356 approach forward and maximise its potential for clinical and scientific neuroimaging.

357 *Clinical diagnosis*

358 Perhaps the more obvious use case for Active Acquisition is in clinical diagnostics and the stratification
359 of individuals into subgroups. Incorporating Active Acquisition could lead to either shorter scanning
360 sessions, or more accurate and more reliable data collection. Multiple imaging modalities are typically
361 collected in a diagnostic clinical scanning session, many of which end up being unnecessary for
362 accurate diagnosis. If the scanning session can be terminated early, when sufficient diagnostic certainty
363 has been reached (as in Scenario 1), there would be a significant reduction in scanning time, reducing
364 patient discomfort and scanning costs. Equally, by optimising the order of the scans (as in Scenario 2),
365 tailored to the targeted disorder, this would potentially remove the need to collect all modalities,
366 leading to the same benefits in terms of time, cost and patient comfort.

367 Alternatively, Active Acquisition could be used to produce more accurate diagnoses and to optimise
368 certain modalities for clinical use that are currently not used in clinical settings. Active Acquisition
369 could make use of scanning time and resources more efficient; collecting repetitions of important scans
370 (until a sufficient signal-to-noise ratio has been reached) or changing the scanning resolution or field-
371 of-view to focus on potential abnormalities. This may be of particular use in relatively low signal-to-
372 noise imaging modalities. For example, the pattern of brain damage presented Scenario 1 (focal
373 ischaemic stroke) is evident even on very low resolution and low signal-to-noise structural scans;
374 however, other neurological conditions may have far more subtle abnormalities and other modalities
375 (e.g., arterial spin labelling, diffusion tensor imaging, resting state or task BOLD scans) have lower
376 signal-to-noise, and may benefit from more spatially focused, repeated data acquisition.

377 A pertinent issue facing neuroimaging research in clinical samples is how to deal with heterogeneity
378 within patient groups; particularly common in chronic neuropsychiatric diseases. The “average” best
379 scanning protocol sequence may well not be optimal at identifying clinically relevant abnormalities in
380 a specific individual. Potentially, different scans may be optimal for a given diagnosis in different
381 individuals and at different points in the natural history of a disease. One major strength of Active

382 Acquisition approaches is that they can more easily locate an individual patient's "sweet-spot" from a
383 large menu of possible scan types/parameters in a time-efficient manner, without having to
384 exhaustively search through all possibilities.

385 *Biomarker discovery*

386 Finding biomarkers that sensitively detect individual variability linked to clinical and scientific
387 questions is an important precursor to improving diagnosis and stratification. The application of Active
388 Acquisition illustrated in Scenario 3 presents a radically different way to achieve this: actively
389 searching for modalities or scanning parameters give abnormal readouts for a single individual. This
390 approach contrasts with the current typical approach to biomarker discovery which can be
391 characterised as choosing a set of modalities prior to scanning that are thought to be related to the
392 clinical question and then assessing them on a large group of patients and controls or subgroups of
393 patients, to provide sufficient statistical power to detect average group differences. Active Acquisition
394 also has the benefit of attempting to focus on modalities only when they are likely to be abnormal for
395 an individual relative to a normative dataset, which is potentially much more powerful than the
396 comparison of group averages, as well as leading intuitively to clinical applications of personalised
397 medicine. Active Acquisition also has the advantage of relying less on relatively arbitrary decisions
398 that lead to a limited number of modalities being acquired, which means that the clinically-relevant
399 sweet-spot for data acquisition is more likely to be found.

400 Active acquisition could also avoid the potential problem of scanning protocols being determined
401 based on biased or inaccurate previous studies. Given the replication 'crisis' in biomedical research,
402 such issues are becoming increasingly recognised as a serious problem in medical imaging. Active
403 optimisation approaches (such as in Scenario 3) involve repeatedly cycling between prediction and
404 hypothesis testing on out-of-sample data, and as such are less susceptible to data overfitting. Equally,
405 active optimisation approaches like these also involve a form of implicit "pre-registration" (Lorenz,
406 Hampshire, and Leech 2017). This makes it harder to engage in certain questionable research practices
407 (e.g., p-hacking, post-hoc hypothesising (Pollock et al. 2017)) that are currently thought to hamper
408 the development of neuroimaging biomarkers.

409 One additional advantage of active optimisation is that it is able to estimate how an individual varies
410 from normality across the whole of the search space, despite only sampling a subset of the modalities
411 tested included in the space. While the gains observed were relatively minor in the current example,
412 where only six modalities organised along one searchable dimension were considered, the potential
413 benefit would grow as the space becomes larger and multidimensional. Using the optimisation
414 algorithm to map out the entire possible space offers the potential for a very rich, but efficiently
415 collected, description of how an individual differs from normality. The search space mapped out could
416 involve observing multiple optima in a given individual and estimating modalities with higher and
417 lower than typical signal. Subsequent offline higher-level modelling (e.g., clustering or other data
418 reduction approaches) could then be applied across individuals to find frequent patterns of abnormality
419 from across all modalities.

420 *Need for different types of normative datasets*

421 One major limiting step to the development of Active Acquisition is the need to have well-
422 characterised variability across individuals in both healthy or 'normal' participants as well as clinical

423 samples and relevant subgroups. Achieving this will require developing large datasets from which to
424 derive estimates of between-individual covariance.

425 Some simpler applications of Active Acquisition could be built with existing normative datasets. For
426 example, when the problem involves deciding when to stop collecting more data because a sufficient
427 signal-to-noise ratio has been reached, increasing confidence in the inferences made from these data.
428 Other approaches could take advantages of new acquisition methods such as the very rapid multi-
429 contrast images at the start of a scan (Skare et al. 2018) or synthetic imaging which are then used to
430 decide whether to collect slower, higher resolution scans. To utilise these types of scans, existing
431 datasets could be utilised to create sufficiently large normative models.

432 However, for other applications, such as when searching across modalities (Scenarios 2 and 3), the
433 benefits of Active Acquisition may be most evident when the space of possible modalities/parameters
434 to be considered is large but structured in some way. Indeed, while at present only a small number of
435 imaging modalities are employed clinically, more modalities could be useful but only for stratifying
436 specific subgroups. An accurate understanding of the covariance between modalities/scan parameters
437 relevant to the clinical or scientific question will be necessary for maximising the benefit from these
438 approaches

439 In Scenario 3, where the optimisation algorithm maps out where an individual is maximally abnormal,
440 understanding the covariance across imaging modalities in a healthy control group (possibly
441 controlling for factors such as age) may suffice. Existing large-scale projects to produce large
442 normative databases have focused on small numbers of modalities collected in large numbers of people
443 (e.g., UK Biobank (Sudlow et al. 2015), Human Connectome Project (Van Essen et al. 2013) and the
444 Cam-CAN dataset presented here). One possible approach is to use meta-analyses of different imaging
445 modalities to try to estimate covariance structure across modalities (capitalising on the fact that
446 different large-scale projects have some shared modalities but also differ from each other). An even
447 better approach would be to have large-scale data collection projects that explicitly seek to quantify
448 covariance across many different imaging modalities/scan parameters. Ideally, this would involve
449 many different representative individuals being scanned, but each with different subsets of
450 modalities/scan parameters; subsequently, a large, comprehensive covariance matrix across
451 individuals can be assembled out of the incomplete datasets from each individual. These normative
452 datasets will allow active searching for how individual patients vary from normality across many
453 modalities, useful for biomarker discovery, without requiring dedicated large multimodal datasets for
454 each clinical condition. Approaches such as Bayesian optimisation with Gaussian processes will allow
455 us to start with relatively few assumptions (i.e., only approximate similarity across modalities near
456 each other in the experimental search space which can be based on health control data); importantly,
457 the approach should work for individuals even when there are areas of the experimental space that
458 deviate from the normative data.

459 There are also likely to be some situations, however, where acquiring targeted multi-modal normative
460 datasets for specific clinical conditions will also be important. For example, when performing
461 diagnostics rather than discovery of biomarkers (more like in Scenario 2). In these situations, bespoke
462 multimodal datasets may be necessary to arrive at a very specific quantification of the covariance
463 between different modalities, in order to accurately guide the sequential decision making. In such

464 situations, particularly, with rare disease groups, acquisition of such datasets would be far more
 465 challenging and may not be practical.

466 *Methodological considerations*

467 All methodological approaches come with costs and benefits; with active acquisition approaches one
 468 concern is that early mismeasurement can lead to serious failures later on. For example, in Scenario 1,
 469 this could result in terminating scans prematurely without collecting sufficient data; or, e.g., in
 470 Scenario 2, this could involve travelling down the wrong branch of the decision tree. In such situations,
 471 important information for diagnosis or biomarker discovery may not be collected. This cost of using
 472 active approaches will be most acute when the underlying covariation between scan modalities is well
 473 understood and the optimal scan type is known. In contrast, the way that we currently collect data in
 474 many exploratory studies (e.g., UK Biobank), it is likely that optimal scans for assessing variability in
 475 an individual are being omitted. This reflects the classic exploration versus exploitation trade off well-
 476 known in computer science.

477 For the benefits of active exploration to be maximised, many choices have to be made regarding the
 478 acquisition function to guide exploration, how to decide when to stop searching, how to quantify
 479 abnormality or predict an individual's classification. We have suggested several simple illustrative
 480 scenarios, but each comes with its own specific challenges and future directions. There is long history
 481 of methodological developments for adaptive studies in clinical situations (Cornfield, Halperin, and
 482 Greenhouse 1969) (Hauskrecht and Fraser 2000)(Alagoz et al. 2010). Future work is needed to
 483 incorporate some of the more sophisticated approaches developed in these other domains to
 484 neuroimaging and ideally combine them multivariate classification and clustering approaches
 485 increasingly commonly used with MRI. In Scenarios 2 and 3, work is needed to understand what
 486 happens when there is not a single optimum modality to maximally quantify abnormality (Scenario 3)
 487 or multiple equally good paths through the decision tree (Scenario 2). Future work is also needed to
 488 evaluate how to robustly quantify the abnormality of an individual's scan, considering the large
 489 number of voxels and possibly heterogeneous or diffuse pathologies. Equally, future work is needed
 490 to develop rapid and robust image pre-processing, so that it can occur in near real-time. Recent
 491 developments in deep learning offer promise, where for example a structural MR image can undergo
 492 an analogue of a complete pre-processing pipeline in a matter of seconds (Cole et al. 2017).

493 Finally, from an MR physics perspective, there are also a number of limitations and challenges.
 494 Actively altering the field-of-view and resolution (as suggested in Scenario 1 where the scan zooms in
 495 on the site of injury) for 3D structural imaging may not have any benefits (in terms of time saved,
 496 increased resolution) given inherent trade-offs between tissue contrast, signal to noise and number of
 497 measurements acquired. However, a similar approach could be taken with other imaging modalities
 498 (e.g., arterial spin labelling, diffusion imaging) where increased signal to noise from restricting the
 499 number of slices or increasing the resolution may be beneficial. Equally, there may be different sources
 500 of information that different resolutions and fields-of-view could acquire (e.g., rapidly assessing
 501 geometry at higher resolution and tissue contrasts at a lower resolution).

502 In summary, here we have presented active acquisition, a novel conceptual approach to how
 503 neuroimaging data could be collected. We have utilised advances in optimisation algorithms and
 504 harnessed large publicly-available neuroimaging databases to develop active acquisition. This

505 approach embeds data analysis into the acquisition process, allowing information to be obtained and
506 employed for making online decisions about the optimal scans or parameters for a given clinical or
507 scientific goal. While active acquisition is still at the embryonic stage, our intention with this
508 manuscript and the illustrative examples contained herein, is to provide the groundwork for future
509 conceptual and experimental work aimed at optimising the acquisition of neuroimaging data for
510 clinical and scientific purposes.

511 **Acknowledgements**

512 Matlab code for the illustrative scenarios presented in this work can be found at
513 <https://github.com/ActiveNeuroImaging/MultimodalActiveAcquisition>. The best way to view the
514 paper is to download the PDF of the paper from the github repository and view it with Adobe Acrobat
515 Reader. Thanks to Dr František Váša for comments on drafts of this manuscript.

516 James Cole is funded by a UKRI Innovation Fellowship and a Wellcome Trust Seed Award in Science.
517 Robert Leech is supported by MRC Research grant MR/R005370/1.

518

519 **References**

- 520 Alagoz, Oguzhan, Heather Hsu, Andrew J. Schaefer, and Mark S. Roberts. 2010. “Markov Decision
521 Processes: A Tool for Sequential Decision Making under Uncertainty.” *Medical Decision
522 Making* 30 (4): 474–83.
- 523 Ashburner, John. 2007. “A Fast Diffeomorphic Image Registration Algorithm.” *Neuroimage* 38 (1):
524 95–113.
- 525 Cole, J. H., S. J. Ritchie, M. E. Bastin, M. C. Valdés Hernández, S. Muñoz Maniega, N. Royle, J.
526 Corley, et al. 2018. “Brain Age Predicts Mortality.” *Molecular Psychiatry* 23 (5): 1385–92.
527 <https://doi.org/10.1038/mp.2017.62>.
- 528 Cole, James H., Matthan WA Caan, Jonathan Underwood, Davide De Francesco, Rosan A. van Zoest,
529 Ferdinand WNM Wit, Henk JMM Mutsaerts, Rob Leech, Gert J. Geurtzen, and Peter Portegies.
530 2018. “No Evidence for Accelerated Ageing-Related Brain Pathology in Treated HIV:
531 Longitudinal Neuroimaging Results from the Comorbidity in Relation to AIDS (COBRA)
532 Project.” *Clinical Infectious Diseases*.
- 533 Cornfield, Jerome, Max Halperin, and Samuel W. Greenhouse. 1969. “An Adaptive Procedure for
534 Sequential Clinical Trials.” *Journal of the American Statistical Association* 64 (327): 759–70.
- 535 Filippini, Nicola, Bradley J. MacIntosh, Morgan G. Hough, Guy M. Goodwin, Giovanni B. Frisoni,
536 Stephen M. Smith, Paul M. Matthews, Christian F. Beckmann, and Clare E. Mackay. 2009.
537 “Distinct Patterns of Brain Activity in Young Carriers of the APOE-E4 Allele.” *Proceedings
538 of the National Academy of Sciences* 106 (17): 7209–14.
- 539 Fritsch, Virgile, Gaël Varoquaux, Benjamin Thirion, Jean-Baptiste Poline, and Bertrand Thirion.
540 2012. “Detecting Outliers in High-Dimensional Neuroimaging Datasets with Robust
541 Covariance Estimators.” *Medical Image Analysis*, Special Issue on the 2011 Conference on

- 542 Medical Image Computing and Computer Assisted Intervention, 16 (7): 1359–70.
543 <https://doi.org/10.1016/j.media.2012.05.002>.
- 544 Good, C. D., I. S. Johnsrude, J. Ashburner, R. N. Henson, K. J. Friston, and R. S. Frackowiak. 2001.
545 “A Voxel-Based Morphometric Study of Ageing in 465 Normal Adult Human Brains.”
546 *NeuroImage* 14 (1 Pt 1): 21–36. <https://doi.org/10.1006/nimg.2001.0786>.
- 547 Hauskrecht, Milos, and Hamish Fraser. 2000. “Planning Treatment of Ischemic Heart Disease with
548 Partially Observable Markov Decision Processes.” *Artificial Intelligence in Medicine* 18 (3):
549 221–44.
- 550 Lancaster, Jenessa, Romy Lorenz, Rob Leech, and James H. Cole. 2018. “Bayesian Optimization for
551 Neuroimaging Pre-Processing in Brain Age Classification and Prediction.” *Frontiers in Aging
552 Neuroscience* 10: 28. <https://doi.org/10.3389/fnagi.2018.00028>.
- 553 Lorenz, Romy, Adam Hampshire, and Robert Leech. 2017. “Neuroadaptive Bayesian Optimization
554 and Hypothesis Testing.” *Trends in Cognitive Sciences* 21 (3): 155–67.
555 <https://doi.org/10.1016/j.tics.2017.01.006>.
- 556 Lorenz, Romy, Ricardo Pio Monti, Inês R. Violante, Christoforos Anagnostopoulos, Aldo A. Faisal,
557 Giovanni Montana, and Robert Leech. 2016. “The Automatic Neuroscientist: A Framework
558 for Optimizing Experimental Design with Closed-Loop Real-Time fMRI.” *NeuroImage* 129
559 (April): 320–34. <https://doi.org/10.1016/j.neuroimage.2016.01.032>.
- 560 Lorenz, Romy, Ines R. Violante, Ricardo Pio Monti, Giovanni Montana, Adam Hampshire, and Robert
561 Leech. 2018. “Dissociating Frontoparietal Brain Networks with Neuroadaptive Bayesian
562 Optimization.” *Nature Communications* 9 (1): 1227. [https://doi.org/10.1038/s41467-018-03657-3](https://doi.org/10.1038/s41467-018-
563 03657-3).
- 564 Modat, Marc. 2012. “Efficient Dense Non-Rigid Registration Using the Free-Form Deformation
565 Framework.” UCL (University College London).
- 566 Poldrack, Russell A., Chris I. Baker, Joke Durnez, Krzysztof J. Gorgolewski, Paul M. Matthews,
567 Marcus R. Munafò, Thomas E. Nichols, Jean-Baptiste Poline, Edward Vul, and Tal Yarkoni.
568 2017. “Scanning the Horizon: Towards Transparent and Reproducible Neuroimaging
569 Research.” *Nature Reviews Neuroscience* 18 (2): 115.
- 570 Shafto, Meredith A, Lorraine K Tyler, Marie Dixon, Jason R Taylor, James B Rowe, Rhodri Cusack,
571 Andrew J Calder, et al. 2014. “The Cambridge Centre for Ageing and Neuroscience (Cam-
572 CAN) Study Protocol: A Cross-Sectional, Lifespan, Multidisciplinary Examination of Healthy

- 573 Cognitive Ageing.” *BMC Neurology* 14 (October). <https://doi.org/10.1186/s12883-014-0204-1>.
- 575 Shahriari, Bobak, Kevin Swersky, Ziyu Wang, Ryan P. Adams, and Nando De Freitas. 2016. “Taking
576 the Human out of the Loop: A Review of Bayesian Optimization.” *Proceedings of the IEEE*
577 104 (1): 148–75.
- 578 Skare, Stefan, Tim Sprenger, Ola Norbeck, Henric Rydén, Lars Blomberg, Enrico Avventi, and
579 Mathias Engström. 2018. “A 1-minute Full Brain MR Exam Using a Multicontrast EPI
580 Sequence.” *Magnetic Resonance in Medicine* 79 (6): 3045–54.
- 581 Smith, Stephen M., Peter T. Fox, Karla L. Miller, David C. Glahn, P. Mickle Fox, Clare E. Mackay,
582 Nicola Filippini, Kate E. Watkins, Roberto Toro, and Angela R. Laird. 2009. “Correspondence
583 of the Brain’s Functional Architecture during Activation and Rest.” *Proceedings of the
584 National Academy of Sciences* 106 (31): 13040–45.
- 585 Smith, Stephen M., Mark Jenkinson, Heidi Johansen-Berg, Daniel Rueckert, Thomas E. Nichols, Clare
586 E. Mackay, Kate E. Watkins, Olga Ciccarelli, M. Zaheer Cader, and Paul M. Matthews. 2006.
587 “Tract-Based Spatial Statistics: Voxelwise Analysis of Multi-Subject Diffusion Data.”
588 *Neuroimage* 31 (4): 1487–1505.
- 589 Smith, Stephen M., Mark Jenkinson, Mark W. Woolrich, Christian F. Beckmann, Timothy EJ Behrens,
590 Heidi Johansen-Berg, Peter R. Bannister, Marilena De Luca, Ivana Drobniak, and David E.
591 Flitney. 2004. “Advances in Functional and Structural MR Image Analysis and Implementation
592 as FSL.” *Neuroimage* 23: S208–19.
- 593 Sudlow, Cathie, John Gallacher, Naomi Allen, Valerie Beral, Paul Burton, John Danesh, Paul Downey,
594 Paul Elliott, Jane Green, and Martin Landray. 2015. “UK Biobank: An Open Access Resource
595 for Identifying the Causes of a Wide Range of Complex Diseases of Middle and Old Age.”
596 *PLoS Medicine* 12 (3): e1001779.
- 597 Van Essen, David C., Stephen M. Smith, Deanna M. Barch, Timothy EJ Behrens, Essa Yacoub, Kamil
598 Ugurbil, and Wu-Minn HCP Consortium. 2013. “The WU-Minn Human Connectome Project:
599 An Overview.” *Neuroimage* 80: 62–79.
- 600 Zhang, Hui, Brian B. Avants, Paul A. Yushkevich, John H. Woo, Sumei Wang, Leo F. McCluskey,
601 Lauren B. Elman, Elias R. Melhem, and James C. Gee. 2007. “High-Dimensional Spatial
602 Normalization of Diffusion Tensor Images Improves the Detection of White Matter
603 Differences: An Example Study Using Amyotrophic Lateral Sclerosis.” *IEEE Transactions on
604 Medical Imaging* 26 (11): 1585–97.
- 605